



Graphene oxide modified forward osmosis membranes with improved hydrophilicity and desalination performance

Xing Wu^{a,b}, Fang Fang^a, Kaisong Zhang^{a,*}

^aKey Laboratory of Urban Pollutant Conversion, Institute of Urban Environment, Chinese Academy of Sciences, Xiamen 361021, China, Tel. +86 0592 6190782; email: ks Zhang@iue.ac.cn (K. Zhang), Tel. +86 0592 6190540; emails: xwu@iue.ac.cn (X. Wu), ffang@iue.ac.cn (F. Fang)

^bUniversity of Chinese Academy of Sciences, Beijing 100049, China

Received 9 February 2017; Accepted 15 July 2017

ABSTRACT

Graphene oxide (GO) was applied to fabricate thin-film nanocomposite forward osmosis (TFN-FO) membranes with improved desalination performance. GO in various concentrations ranging from 0.0005 to 0.06 wt% was added to the aqueous phase solution before the interfacial polymerization process. GO modified FO membranes were characterized and the desalination performance was investigated. Results indicated that the TFN-FO membranes formed a typical “ridge-and-valley” structure, achieved a lower reverse solute flux, and showed improvements on membrane hydrophilicity, water fluxes, and salt rejection. When 2 mol·L⁻¹ of NaCl and 10 mmol·L⁻¹ NaCl were used as the draw solution and the feed solution, respectively, the water flux of the membrane modified by 0.005 wt% GO reached the climax at 8.59 L·m⁻²·h⁻¹ (LMH) in the active layer facing the feed solution mode (the active layer facing the draw solution), which increased 55.6% compared with that of the pristine membranes. Moreover, the desalination performance of TFN-FO was compared with the pristine FO membranes under different operating conditions with various draw solution concentrations, cross-flow rates and orientations of membranes. Results showed that the TFN-FO membranes had enhanced desalination performance under all operating conditions in this study. The 0.005 wt% GO nanosheet was the optimal and such low contents of GO are promising for a wide-scale industrial application.

Keywords: Forward osmosis; Graphene oxide; Desalination; Interfacial polymerization

1. Introduction

Forward osmosis (FO) has been gaining increasing popularity in the water industry, especially, useful for seawater desalination, wastewater management, and other industrial applications such as ethanol concentration, protein concentration, algae separation, and power generation [1–3]. Known for their lower energy expenditure and effectiveness in alleviating membrane fouling, FO membranes are more competitive compared to traditional pressure-driven membranes, for instance, reverse osmosis (RO) membranes and nanofiltration membranes [4,5]. Apart from the advantages, however,

it is still challenging to produce an advanced FO membrane with high water fluxes, high rejection and reduced internal concentration polarization (ICP) [6–8].

A significant development of FO membrane materials was witnessed in the last decades, changing from nitrocellulose to recent cellulose acetate (CA) and thin-film composite (TFC) [1,9]. Compared with CA membranes produced through phase inversion, TFC membranes prepared by the interfacial polymerization process have advantages including better mechanical strength and lower ICP [9–11]. Moreover, a TFC-FO membrane can be divided into a substrate membrane and an active layer, making it more flexible for membrane preparation, and much preferable for the market. Currently, polysulfone (PSf) is widely used to prepare TFC membranes. However, poor permeability of

* Corresponding author.

PSf-based membranes still remains a serious problem that cannot be neglected [11].

Membrane modification is one of the most effective approaches to enhancing membrane performance. Inorganic nanomaterials including zeolite, titanium dioxide, and silicon dioxide were widely utilized as membrane modifiers [12,13]. Recently, carbon nanomaterials such as carbon nanotubes (CNTs) and graphene oxide (GO) have gained increasing attention as modifier materials in membrane fabrication. Compared with CNTs, GO shows better mechanical performance, larger surface area, and natural hydrophilicity; hence potentially a more efficient membrane modifier [14–16]. Ganesh et al. [17] reported that GO modified PSf ultrafiltration (UF) membranes showed enhancements in both water fluxes and sodium sulfate rejection. Ionita et al. [15] reported that incorporating GO with PSf could improve the thermal and mechanical performance of membranes. However, previous studies indicated that the required amount of GO was rather large (over 0.25 wt%) when GO was added into UF membranes [15,18]. High contents of GO required would carry a relatively high financial cost if GO were to be used as a membrane modifier. Some researchers focused on embedding GO directly into the active layer of TFC membranes. Results showed improvements in membrane performance such as water fluxes, salt rejection and antifouling [19,20]. However, most previous studies on GO modified thin-film nanocomposite (TFN) membranes were associated with pressure-driven membranes. Only a few investigations looked into the influences of GO as a surface modifier for FO membranes. Moreover, the aggregation of GO was reported when the amount of GO exceeded 0.06 wt% [20], resulting in poor desalination performance. Therefore, it is critical to identify the optimal amount of GO needed when using it as a membrane modifier.

In the process of fabricating TFN-FO membranes, GO was embedded into the aqueous phase solution before the interfacial polymerization process to fully utilize the hydrophilic functional groups of GO. One principal objective of this study is to systematically investigate the feasibility of GO to modify osmosis-driven membranes. The other objective is to optimize the required amount of GO, resulting in a lower financial and environmental cost for GO manufacturing.

2. Experimental setup

2.1. Materials

Polysulfone (PSf, Solvay P3500) purchased from BASF Co., Ltd. (China), polyvinylpyrrolidone (PVP, K30) purchased from Sigma-Aldrich, China, and 1-methyl-2-pyrrolidinone (NMP, ≥99%) purchased from Sinopharm Chemical Reagent Co., Ltd. (China) were used for the preparation of PSf substrate membranes. GO (DK Nano technology Co., Ltd., China) with 30%–40% oxygen-containing groups were applied as the membrane modifier. Trimesoyl chloride (TMC, 98%) and *m*-phenylenediamine (MPD) were purchased from Aladdin (China). *n*-Hexane (99%) was supplied by Sinopharm Chemical Reagent Co., Ltd. (China) and was used for the interfacial polymerization. Sodium chloride (NaCl) bought from Sinopharm Chemical Reagent Co., Ltd. (China) was utilized to test membrane performance.

2.2. Preparation of substrate membranes

The PSf UF membrane was fabricated and used as the substrate of FO membranes. The casting solution was prepared by dissolving 0.5 wt% of PVP and 17.5 wt% of PSf into 82 wt% NMP solution. The casting solution was spread on a clean glass plate at a knife height of 175 μm, and was then immediately transferred into a water bath. The substrate membrane showed a water flux of 367 L·m⁻²·h⁻¹ (LMH), and 99.4% rejection of 1 g·L⁻¹ bovine serum albumin under the pressure of 0.1 MPa in a dead-end filtration testing system.

2.3. Preparation of GO modified FO membranes

Different amounts of GO that are listed in Table 1 were dissolved into the deionized (DI) water and were ultrasonicated for 3 h under a sonication power of 500 W. Then, 2.0 wt% MPD was added to the GO solution. Through the interfacial polymerization, a dense active layer of a FO membrane was formed on the substrate membrane. Firstly, 2.0 wt% MPD aqueous solution containing 0–0.06 wt% of GO was poured onto the surface of the substrate membrane for 2 min. Excess MPD aqueous solution was removed by a rubber roller. After that, 0.1 wt% TMC dissolved in *n*-hexane was poured onto the surface of the membrane. After 1 min, the TMC solution was drained off and the pure *n*-hexane was poured on the membrane to remove excess TMC solution. Later, the membrane was stored in an oven at 60°C for 8 min. At last, the membrane was stored in a DI water bath for future use. After the membrane preparation procedures were complete, membranes were named as F0, F1, F2, F3, F4, F5, and F6 based on the amounts of GO in MPD solution.

2.4. Characterization of GO nanosheets and FO membranes

The phase structure of the GO powder employed in this experiment was investigated using a X-ray diffractometer (X'Pert PRO, PANalytical B.V., the Netherlands) with 2θ ranging from 10° to 50°. The XRD measurement of GO was carried out under the Cu Kα radiation wavelength (λ = 1.54 Å) at 40 kV and 30 mA. The average interlayer space was determined by Bragg's law using the following equation [21]:

$$n\lambda = 2d \sin \theta \quad (1)$$

Table 1
The compositions of solution for the interfacial polymerization

Membrane	Concentration of GO in MPD (wt%)	Concentration of MPD (wt%)	Concentration of TMC (wt%)
F0	0	2.0	0.1
F1	0.0005	2.0	0.1
F2	0.001	2.0	0.1
F3	0.0025	2.0	0.1
F4	0.005	2.0	0.1
F5	0.02	2.0	0.1
F6	0.06	2.0	0.1

where n is an integer (1, 2, 3...), d is the space between diffracting planes, θ is the incident angle, and λ is the wavelength of the beam.

Attenuated total reflectance Fourier transform infrared spectroscopy (ATR-FTIR, Nicolet iS10, Thermo Fisher Scientific, USA) was used to observe the GO nanosheets, with the wavenumbers ranging from 1,000 to 4,000 cm^{-1} at a resolution of 4.0 cm^{-1} . Raman spectra of the GO aqueous solution were collected using a LabRAM Aramis (HORIBA Jobin Yvon) confocal micro-Raman system.

In order to investigate the hydrophilicity of membranes, a sessile drop analysis system (DSA100, KRUSS, Germany) was applied to measure the contact angles of membranes. The contact angles were tested immediately after placing a drop of DI water on the surface of membranes. Five locations in each sample were randomly selected to calculate the average contact angle. Before stuck onto glass slides, all membranes were dried in a freeze dryer for 48 h. The functional groups of membrane surface were characterized by ATR-FTIR, which was used to identify the presence of GO. ATR-FTIR spectra ranged from 1,000 to 4,000 cm^{-1} at a resolution of 4.0 cm^{-1} . Before investigation, membrane samples were kept at room temperature for 24 h to dry. Moreover, a field emission scanning electron microscope (FESEM, HITACHI S-4800, Japan) system was applied to observe views of the surfaces and the cross sections of the FO membranes. Before coated with gold, membrane samples were dried in an oven for 48 h at 80°C. The accelerating voltage of FESEM was 5 kV.

2.5. Evaluation of desalination performance of FO membranes

Salt rejections (R) of the pristine FO and the GO modified FO membranes were measured in a bench-scale RO filtration test system. The active area of each membrane sample was 33.8 cm^2 . 10 L of 20 $\text{mmol}\cdot\text{L}^{-1}$ sodium chloride solutions were selected as the feed solution. The system was kept at 0.25 MPa and with a cross-flow rate of 45 $\text{L}\cdot\text{h}^{-1}$. R was calculated by the following equation:

$$R = \left(1 - \frac{C_p}{C_f} \right) \times 100 \quad (2)$$

where C_p and C_f are NaCl concentrations in the permeate solution and the feed solution, respectively, which could be calculated by the conductivity of solution.

All membranes were also tested in the FO test system (Fig. 1) in the active layer facing the feed solution (AL-FS) mode, which was characterized as the active layer facing the feed solution. Total active membrane area was 33.8 cm^2 . 2 L of 2 $\text{mol}\cdot\text{L}^{-1}$ NaCl were used as the draw solution while 2 L of 10 $\text{mmol}\cdot\text{L}^{-1}$ NaCl as the feed solution. The flow rates of both the draw solution and the feed solution were maintained at 20 $\text{L}\cdot\text{h}^{-1}$, while the temperature was kept at room temperature. A digital weight balance and a conductivity meter were used to evaluate the weight change of the draw solution and the conductivity change of the feed solution, respectively. The water flux (J_w) and the reverse solute flux (J_s) were measured after the FO system reached the steady state, which was 45 min from the beginning. Both J_w and J_s were measured every 15 min and were repeated five times to calculate the average value.

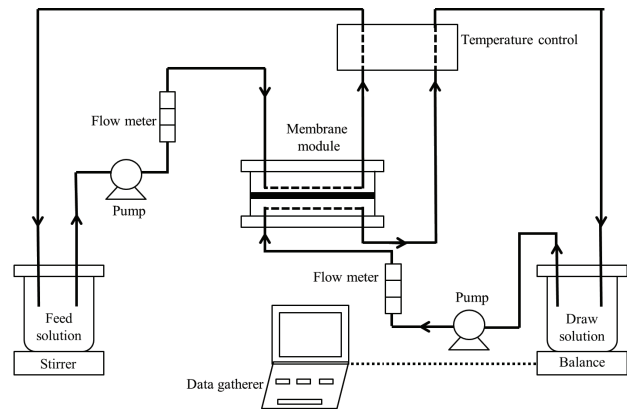


Fig. 1. Setup of a forward osmosis testing system.

Following equations were used to calculate the water flux and the reverse solute flux, respectively.

$$J_w = \frac{\Delta V}{\Delta t \cdot A_m} \quad (3)$$

$$J_s = \frac{\Delta(C_t V_t)}{\Delta t \cdot A_m} \quad (4)$$

where ΔV is the volume of permeated water (L), A_m is the membrane area (m^2), Δt is the permeation time (h), C_t is the concentration of NaCl at the end of permeation time, and V_t is the volume of permeated water at the end of permeation time (L).

2.6. Filtration optimization of FO membranes

The desalination performance of FO filtration is related to the operating conditions, including cross-flow rates, membrane orientations and draw solution concentrations [22]. The GO modified membrane with the best desalination performance tested in Section 2.5 (e.g., high water flux and high salt rejection) was selected to be compared with the pristine FO membrane under various application conditions, including different cross-flow rates (15, 20 and 30 $\text{L}\cdot\text{h}^{-1}$), membrane orientations in both the AL-FS and the AL-DS (the active layer facing the draw solution) and different draw solution concentrations (1, 2, and 4 $\text{mol}\cdot\text{L}^{-1}$).

3. Results and discussion

3.1. Characterization of GO and FO membranes

Fig. 2(a) illustrates the phase structures of the GO nanosheets. The peak at $2\theta = 10.46^\circ$ was attributed to the (001) reflection of GO, indicating that the interlayer space of GO was 8.45 Å. Compared with the interlayer space of graphite, which was reported to be approximately 3.37 Å [23], the increased interlayer distance between GO nanosheets was caused by the embedded oxygen-containing functional groups on the surface of GO nanosheets. Fig. 2(b) presents typical functional groups around the surface of GO nanosheets. It could be observed that there was a peak at 1,051 cm^{-1} due to the C–O bonds in epoxy groups, a peak at 1,400 attributed to the =C–H bands, and a peak at 1,613 cm^{-1} attributed to the un-oxidized sp^2 C=C bonds in the carbon

lattice. A peak was also found at $1,720\text{ cm}^{-1}$, associated with the presence of carbonyl and stretching bands of carboxylic groups. One other peak presented at $3,432\text{ cm}^{-1}$ was associated with hydroxyl groups [20,24,25]. The Raman spectra of GO nanosheets (Fig. 2(c)) shows the typical two peaks at $1,337\text{ cm}^{-1}$ (D band) and $1,592\text{ cm}^{-1}$ (G band), and the intensity ratio of D band and G band was 0.96, confirming the presence of oxygen-containing groups on GO nanosheets [20]. These results together proved the presence of oxygen-containing functional groups on GO, which would improve the hydrophilicity of GO.

Fig. 3 shows the ATR-FTIR spectra of GO modified membranes, with wavenumbers ranging from $1,000$ to $4,000\text{ cm}^{-1}$.

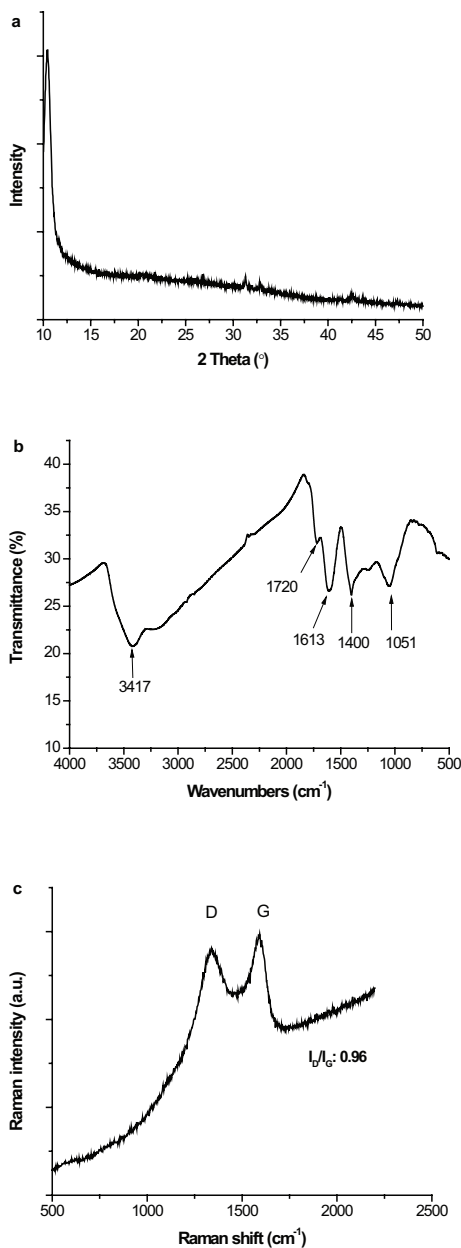


Fig. 2. (a) X-ray diffraction pattern of GO nanosheets, (b) ATR-FTIR spectra of GO nanosheets, and (c) Raman spectra of GO nanosheets.

It was observed that all FO membranes prepared by the interfacial polymerization of MPD and TMC had similar peaks at specific wavenumbers. The peaks at $1,150$, $1,294$, and $1,321\text{ cm}^{-1}$ were associated with the asymmetric sulfur dioxide stretching vibration and symmetry stretching vibration. The peaks at $1,487$ and $1,585\text{ cm}^{-1}$ were related to aromatic in-plane ring bend stretching vibration. The formation of the peak at $1,649\text{ cm}^{-1}$ was attributed to the amide carbonyl ($\text{C}=\text{O}$) stretching vibration of the amide I [20,26]. At a wavenumber of $1,649\text{ cm}^{-1}$, the intensity of the peaks tended to grow with GO concentrations. This improvement was potentially associated with the new amide chains formed by the interaction between hydroxyl groups of GO and amino groups of MPD, proving the presence of GO on the membrane surface. Similar results were reported by previous researchers [26,27]. Another evidence that confirmed the presence of GO on membrane surface was a peak at $3,367\text{ cm}^{-1}$, which was associated with the hydroxyl stretching vibration existing on GO nanosheets [26]. With increasing GO concentrations, the transmittance peaks of membranes at the wavenumber of $3,367\text{ cm}^{-1}$ became more apparent, suggesting that GO nanosheets were embedded on the surface of the active layers of FO membranes.

Water contact angles were measured to evaluate the hydrophilicity of FO membranes. It could be observed that the PSf substrate membrane had the highest contact angle of 87.8° (Fig. 4). Moreover, while the GO concentrations rose from 0 to 0.06 wt%, the contact angles declined from 72.9° to 57.6° , witnessing almost a 21% reduction. This result suggested that the GO modified membranes were more hydrophilic than membranes without GO, which was due to the presence of hydroxyl groups on the surface of GO modified membranes confirmed by the results of ATR-FTIR.

Fig. 5 illustrates the FESEM images of FO membrane cross sections. A computer software, "Nano Measurer", was applied to measure the width of polyamide active (PA) layers in SEM images. By comparing the width of PA layers to the scale in SEM images, the thickness of the PA layer of a FO membrane could be determined. 20 locations were selected

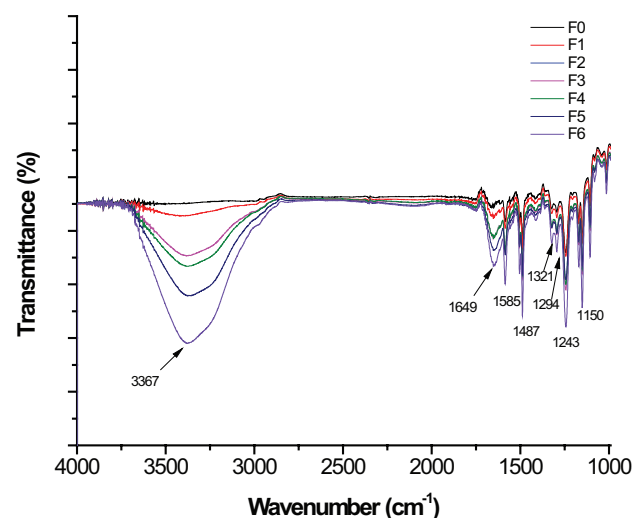


Fig. 3. ATR-FTIR spectra of FO membranes modified with different GO concentrations.

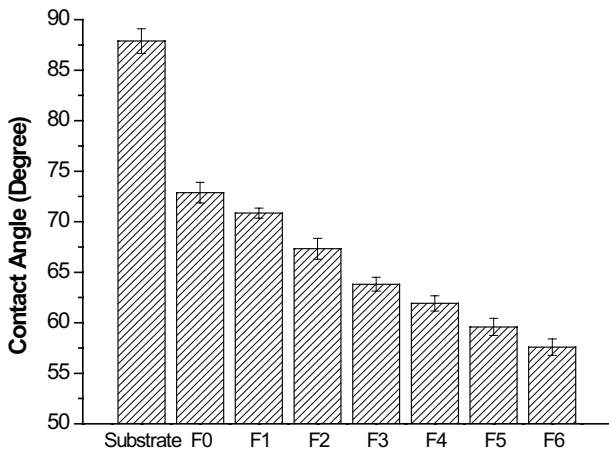


Fig. 4. Contact angles of PSf substrate, F0, F1, F2, F3, F4, F5, and F6 membranes.

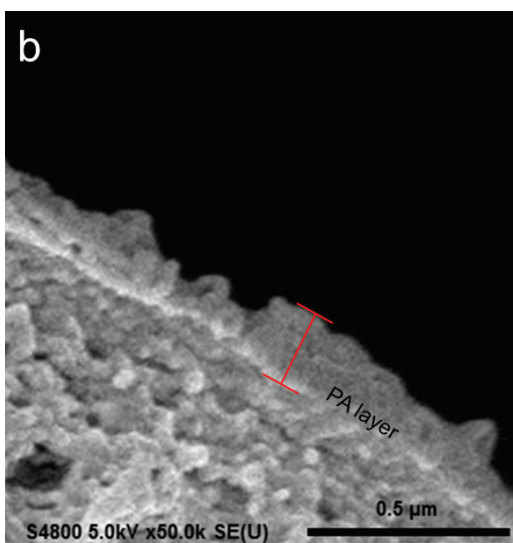
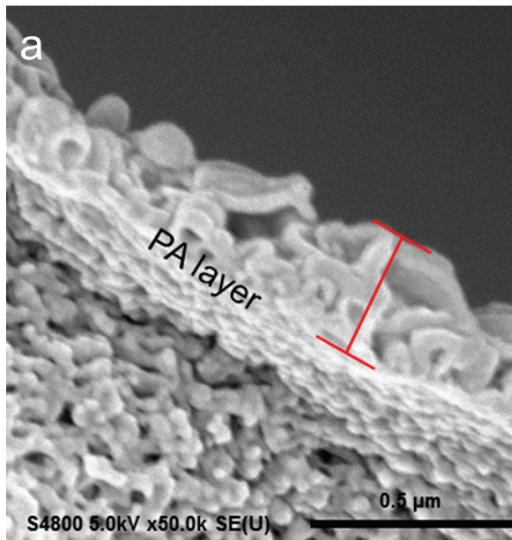


Fig. 5. FESEM of cross sections of (a) F0 and (b) F4 membranes.

from each SEM image to calculate the average thickness of a PA layer. It could be observed from Fig. 5 that, the thickness of the dense polyamide layer of the pristine FO membrane was approximately 226 nm while the average thickness of F4 membrane decreased to 153 nm. This reduction was potentially due to the interference of GO in the interfacial polymerization process. It was believed that during the interfacial polymerization process, the dense polyamide layer tended to build up when the MPD diffused into the organic side of the interface [28]. When GO nanosheets embedded, they tend to horizontally arrange on the membrane surface [19,29]. These GO nanosheets prevented MPD from further diffusing, and therefore impeded the reaction between MPD and TMC, resulting in a thinner PA layer. Moreover, according to the results of ATR-FTIR and previous studies [26,30,31], besides the hydrogen bonds between GO and MPD, the carboxylic groups of GO also reacted chemically with the amino groups of MPD, and with the acylchloride groups of TMC (Fig. 6). As a result, the amounts of amino groups and chloride groups for the interfacial polymerization declined, and the extent of the interfacial polymerization was weakened. Besides reducing the thickness of PA layers, GO also affected the surface structure of PA layers of FO membranes. It was observed from Fig. 7 that all these FO membranes prepared through the interfacial polymerization showed similar surface morphologies, which was known as the ridge-and-valley structure [19]. There was a crosslinking network above the globular structures in all samples. However, the membrane surface of F6 was not uniform, which was potentially due to the effects of high-concentration GO in the interfacial polymerization process [29].

3.2. Desalination performance of FO membranes

It was observed that water fluxes of membranes modified by GO were higher than that of the pristine FO membrane, ranging from 2.4% to 56.1% (Fig. 8(a)). The water fluxes of membranes kept rising with increasing GO concentrations, and reached the maximum of 8.59 LMH when the GO concentration was 0.005 wt%. This was mainly due to the fact that the embedded GO nanosheets increased the hydrophilicity of membrane surfaces, which was confirmed by the results of ATR-FTIR and the contact angle experiments. The hydrophilic surface improved the adsorption of water molecules on the membrane surfaces through interactions between hydrogen bonds, and eventually enhanced the transportation of water molecules into membranes [17,19,20]. However, when the GO concentration was higher than 0.005 wt%, the water flux decreased but still above the F0 level. This was a combination of the opposite effects of increased hydrophilicity on membrane surfaces and GO aggregation at a high concentration. According to the results of contact angles, the hydrophilicity of membranes increased with growing GO concentrations, leading to a higher water flux. Moreover, thinner PA layers of GO modified membranes also contributed to the enhancement of water fluxes [31]. As a result, compared with the F4 membrane, F5 and F6 membranes had lower water fluxes. Fig. 8(b) illustrates the influence of GO on the reverse solute flux of membranes. Similar to the result of water fluxes, no significant differences were observed between the F0 and the F1 membranes, which was due to the negligible influence of

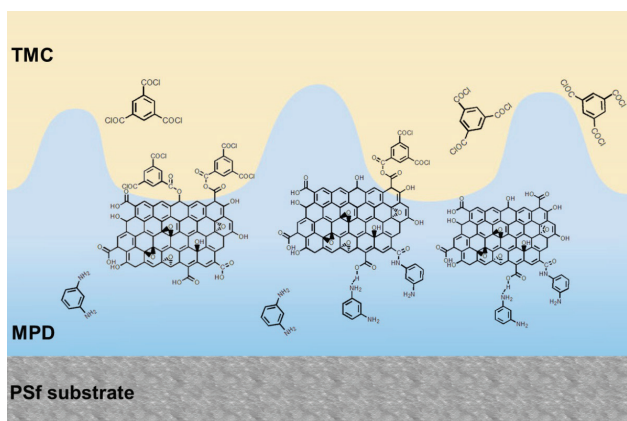


Fig. 6. Reactions of GO with MPD and GO with TMC.

the small amount of GO on these FO membranes. When the concentrations of GO increased from 0.001 to 0.02 wt%, the reverse solute fluxes became lower than that of the pristine FO membrane, indicating the desalination performance of membranes was comprehensively improved by GO. When embedded with GO, the PA layers of FO membranes grew denser, leading to an improved separation performance [31].

Regarding sodium chloride rejection, the tendency of the salt rejection changed inversely with the tendency of the reverse solute flux (Fig. 8(c)). It was observed that the NaCl rejection of 0.02 wt% GO modified membrane (F4) grew from 83.7% to 89.5%. This enhanced salt rejection was due to the arrangement of GO nanosheets on the active layer that became denser [29,31]. However, when the GO concentration increased to 0.06 wt%, the salt rejection decreased to 78.2% due to the interaction between GO and MPD, as well as the interaction between GO and TMC. The interactions impeded the interfacial polymerization process and influenced the formation of the active layer, resulting in a weaker desalination performance of membranes. It could be found that 0.06 wt% GO concentration deteriorated the desalination performance of FO membranes. The result from Fig. 8 also indicated that there was no obvious “trade-off” phenomenon between the water fluxes and the salt rejection of GO modified membranes. These results altogether suggested that the improvement of desalination performance was comprehensive, meaning both water fluxes and salt rejection were enhanced.

3.3. FO filtration optimization

According to the result of the desalination performance test, it was found that the F4 membrane showed the highest water flux and improved salt rejection. Therefore, F4 membrane was selected to be compared with the pristine FO membrane under different filtration conditions. Fig. 9 illustrates the water fluxes of the pristine FO membrane and F4 membrane at different cross-flow rates. 2 L of 2 mol·L⁻¹ NaCl and 2 L of 10 mmol·L⁻¹ NaCl were used as the draw solution and the feed solution, respectively, with the active layer of the membrane facing the feed solution. It was observed that during the 300 min test, water fluxes of F4 were higher than that of the F0 membrane at the same cross-flow rate. In addition, water fluxes of both two membranes had similar tendencies, which showed that higher the cross-flow rates

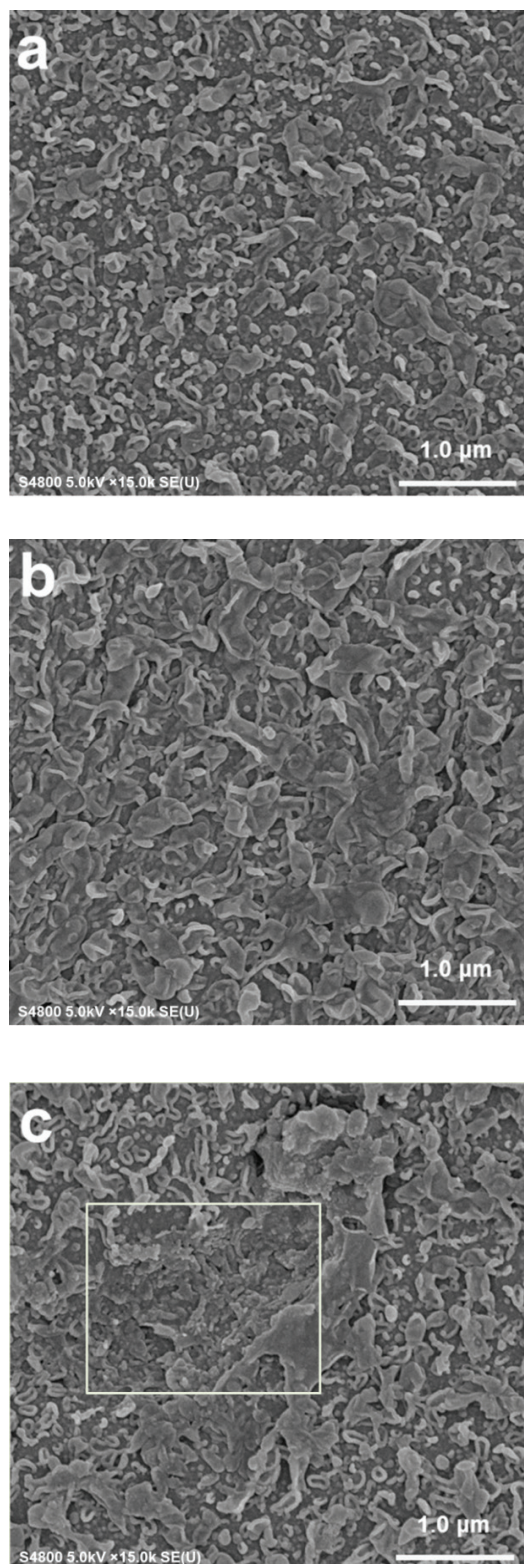


Fig. 7. FESEM of surfaces of (a) F0, (b) F4, and (c) F6 membranes.

of FO filtration were, higher the water fluxes would be. The major reason was that a larger shear force provided by higher rates reduced the aggregation of NaCl on the surface of membranes. This ultimately mitigated the external concentration

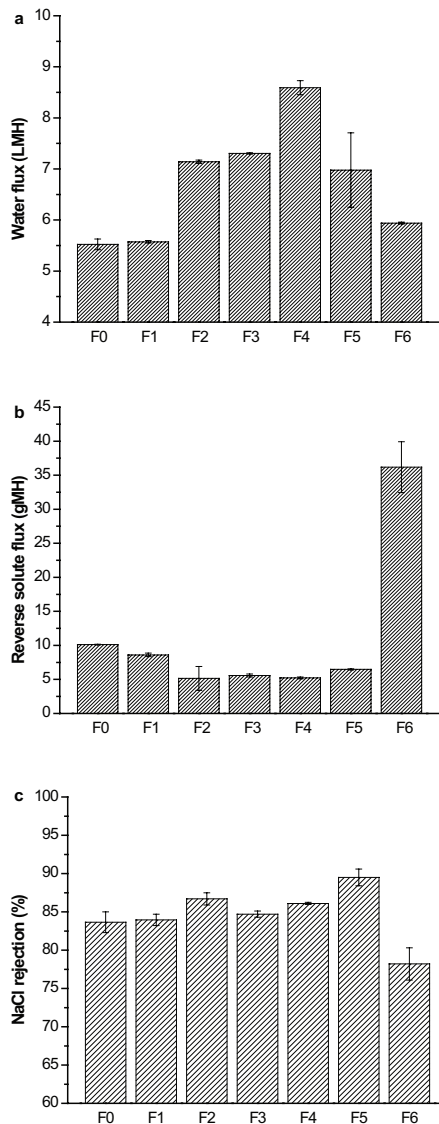


Fig. 8. Desalination performance of membranes with different GO concentrations: (a) water fluxes of membranes, (b) reversed solute fluxes of membranes, and (c) salt rejection of membranes. Water fluxes and reversed solute fluxes were measured in the FO operating conditions: the AL-FS mode, 2 mol·L⁻¹ NaCl solution as the draw solution and 10 mmol·L⁻¹ NaCl solution as the feed solution. Rejections were tested under the RO operating conditions: 20 mmol·L⁻¹ NaCl solution as the feed solution, the pressure was 0.25 MPa, and the cross-flow rate was 45 L·h⁻¹.

polarization of membranes, and increased the water fluxes of membranes. Compared with the beginning of the filtration, the water flux underwent different levels of decrease at the end of the test. It could also be observed that when the rates of cross-flow increased from 15 to 30 L·h⁻¹, the percentages of water flux decrease dropped from 14.0% to 7.4% in the pristine FO membranes. In comparison, the dropping percentages of F4 membranes were smaller, which were 10.2% for 15 L·h⁻¹, 8.9% for 20 L·h⁻¹ and 5.1% for 30 L·h⁻¹, respectively. This was attributed to the increased hydrophilicity of membrane surface which led to an easier adsorption of water molecules, and reduced the aggregation of NaCl on

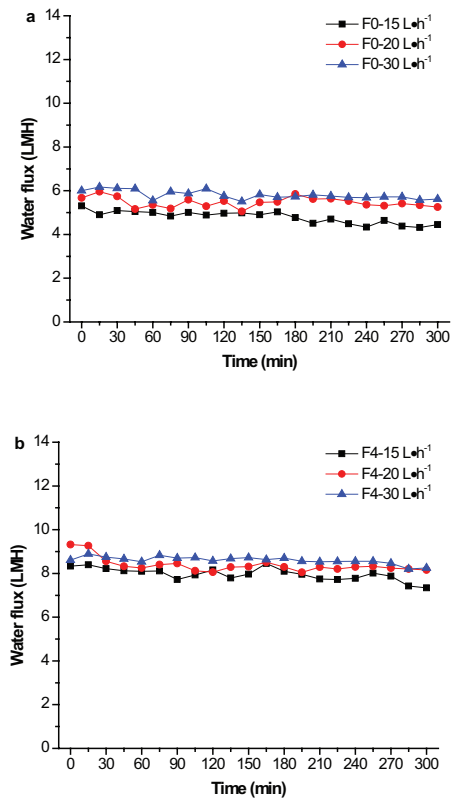


Fig. 9. Water fluxes of membranes with different cross-flow rates: (a) water fluxes of the F0 membrane, and (b) water fluxes of the F4 membrane. The FO operating conditions: the AL-FS mode, 2 mol·L⁻¹ NaCl solution as the draw solution, and 10 mmol·L⁻¹ NaCl solution as the feed solution.

the membrane surface. Moreover, it was also observed that the increase of water fluxes was slight when the cross-flow rates grew, which was in line with other studies stating that the influence of external concentration polarization was not dominant for water fluxes of membranes [32].

Fig. 10 shows the average water fluxes of the F0 and the F4 membranes before and after 300 min filtration test with different membrane orientations. The water flux showed in this figure was calculated by the average value of four duplicate samples (Table S1). 2 mol·L⁻¹ NaCl was used as the draw solution and 10 mmol·L⁻¹ NaCl was employed as the feed solution. The cross-flow rate was maintained at 20 L·h⁻¹. It could be observed that both the F0 membrane and the F4 membrane witnessed a slight reduction of water flux during the 300 min water flux test in both AL-DS and AL-FS orientations. The water flux reduction for the F0 membrane was 7.7% in AL-FS mode and 12.7% in AL-DS mode, while the water flux reduction for the F4 membrane was 10.5% in AL-FS mode and 11.1% in AL-DS mode. Compared with membranes in AL-FS orientation, membranes in AL-DS orientation had a more significant drop of water fluxes. This was due to the high water fluxes of membranes in the AL-DS mode, which enhanced the dilution of the draw solution and the concentration of the feed solution and finally reduced the osmotic pressure across the FO membranes. Overall, it was found that the GO modified FO membrane always showed greater water fluxes than that of the pristine membrane when

examined under identical conditions. Based on the results acquired, it could be concluded that GO was an effective modifier to be used on the surface of FO membranes.

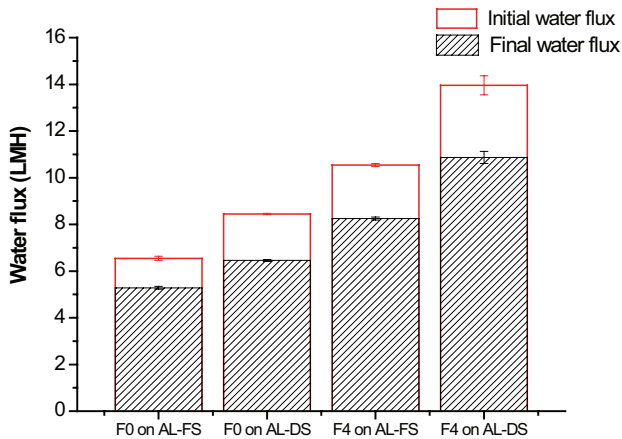


Fig. 10. Water fluxes of the F0 and the F4 membranes with different membrane orientations before and after 300 min filtration test. The FO operating conditions: 2 mol·L⁻¹ NaCl solution as the draw solution, 10 mmol·L⁻¹ NaCl solution as the feed solution, and the cross-flow rate was 20 L·h⁻¹.

Fig. 11 shows the water fluxes of the pristine FO membrane and F4 membrane using different concentrations of the draw solutions. As the concentrations of the draw solutions increased, both membranes showed higher water fluxes, which could be attributed to the higher osmotic pressure difference found over the membranes [33]. In addition, higher water flux was found in F4 membrane compared with the pristine FO membrane at a same draw solution concentration. The water fluxes showed no obvious decrease during the 300 min test. This could be explained by the insignificant impacts of the water fluxes on the reduction of osmotic pressure when the water fluxes were not high. In the meantime, reverse solute fluxes went up as the concentration of draw solution increased (Figs. 11(c) and (d)), which was associated with the high salt concentration gradient passing through the active layer of membranes [33]. Compared with the percentages of water fluxes increase, the percentages of reverse solute fluxes increase were noticeably larger. When the concentrations of the draw solution rose from 2 to 4 mol·L⁻¹, the percentages of water fluxes increase were 77% for the F0 membrane and 45% for the F4 membrane. The reverse solute flux, however, increased 162% in the F0 membrane and 276% in the F4 membrane. For a high-quality FO membrane, both high water flux and low reverse solute flux are desired. Therefore, according to these results, it was suggested that

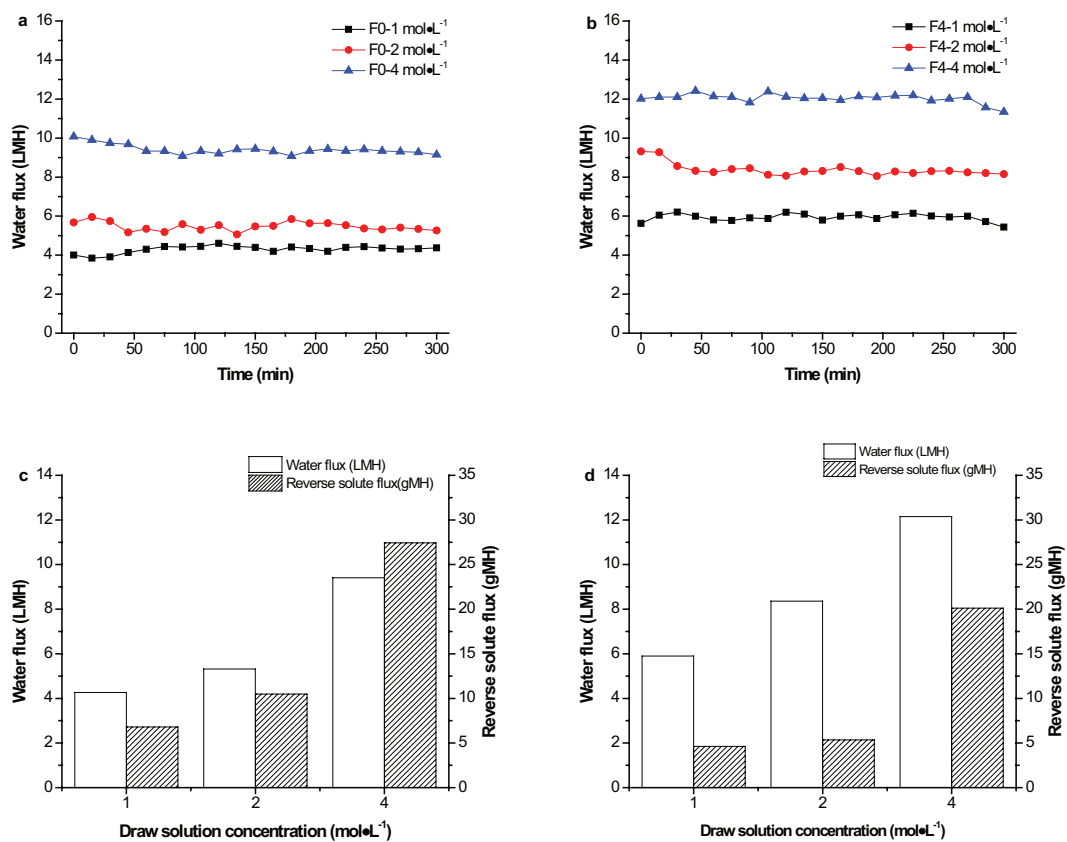


Fig. 11. Water fluxes and reverse solute fluxes of membranes with different concentrations of draw solutions: (a) water fluxes of the F0 membrane overtime, (b) water fluxes of the F4 membrane over time, (c) average water fluxes and reverse solute fluxes of the F0 membrane, and (d) average water fluxes and reverse solute fluxes of the F4 membrane. Water fluxes and reversed solute fluxes were measured under the FO operating conditions: the AL-FS mode, 10 mmol·L⁻¹ NaCl solution as the feed solution, and the cross-flow rate was 20 L·h⁻¹.

when the draw solution concentration was 2 mol·L⁻¹, both the F0 membrane and the F4 membrane showed higher desalination efficiency.

4. Conclusions

FO membranes were prepared and modified by GO dispersed in the MPD solution before the interfacial polymerization. The GO modified membranes showed improvements on hydrophilicity, sodium chloride rejection and water fluxes when the concentrations of embedded GO were adjusted from 0.001 to 0.02 wt%. The key factor to promote desalination performance is the GO concentration. Among all membranes that were tested, the membranes modified by 0.005 wt% of GO nanosheets showed the optimized desalination performance.

Acknowledgements

The author K.Z. would like to thank the Royal Academy of Engineering, UK, for a research exchange with China/India scheme. X.W. would like to thank Ms. Siqian Tu for English editing. The authors gratefully acknowledge the financial support by Xiamen Municipal Bureau of Science and Technology (3502Z20131159) and Bureau of International Cooperation, CAS. The authors are also grateful to the reviewers for their helpful and insightful comments.

References

- [1] S. Zhao, L. Zou, C.Y. Tang, D. Mulcahy, Recent developments in forward osmosis: opportunities and challenges, *J. Membr. Sci.*, 396 (2012) 1–21.
- [2] E.M. Garcia-Castello, J.R. McCutcheon, Dewatering press liquor derived from orange production by forward osmosis, *J. Membr. Sci.*, 372 (2011) 97–101.
- [3] B.E. Logan, M. Elimelech, Membrane-based processes for sustainable power generation using water, *Nature*, 488 (2012) 313–319.
- [4] Y. Sun, L. Xue, Y. Zhang, X. Zhao, Y. Huang, X. Du, High flux polyamide thin film composite forward osmosis membranes prepared from porous substrates made of polysulfone and polyethersulfone blends, *Desalination*, 336 (2014) 72–79.
- [5] T.-S. Chung, X. Li, R.C. Ong, Q. Ge, H. Wang, G. Han, Emerging forward osmosis (FO) technologies and challenges ahead for clean water and clean energy applications, *Curr. Opin. Chem. Eng.*, 1 (2012) 246–257.
- [6] Y. Huang, H. Jin, P. Yu, Y. Luo, Polyamide thin-film composite membrane based on nano-silica modified polysulfone microporous support layer for forward osmosis, *Desal. Wat. Treat.*, 57 (2016) 20177–20187.
- [7] K. Lutchmiah, A.R. Verliefe, K. Roest, L.C. Rietveld, E.R. Cornelissen, Forward osmosis for application in wastewater treatment: a review, *Water Res.*, 58 (2014) 179–197.
- [8] M. Qasim, N.A. Darwish, S. Sarp, N. Hilal, Water desalination by forward (direct) osmosis phenomenon: a comprehensive review, *Desalination*, 374 (2015) 47–69.
- [9] N. Akther, A. Sodiq, A. Giwa, S. Daer, H.A. Arafat, S.W. Hasan, Recent advancements in forward osmosis desalination: a review, *Chem. Eng. J.*, 281 (2015) 502–522.
- [10] S. Zhang, K.Y. Wang, T.-S. Chung, H. Chen, Y.C. Jean, G. Amy, Well-constructed cellulose acetate membranes for forward osmosis: minimized internal concentration polarization with an ultra-thin selective layer, *J. Membr. Sci.*, 360 (2010) 522–535.
- [11] N.Y. Yip, A. Tiraferri, W.A. Phillip, J.D. Schiffman, M. Elimelech, High performance thin-film composite forward osmosis membrane, *Environ. Sci. Technol.*, 44 (2010) 3812–3818.
- [12] D. Emadzadeh, W.J. Lau, T. Matsuura, A.F. Ismail, M. Rahbari-Sisakht, Synthesis and characterization of thin film nanocomposite forward osmosis membrane with hydrophilic nanocomposite support to reduce internal concentration polarization, *J. Membr. Sci.*, 449 (2014) 74–85.
- [13] D. Emadzadeh, W.J. Lau, T. Matsuura, N. Hilal, A.F. Ismail, The potential of thin film nanocomposite membrane in reducing organic fouling in forward osmosis process, *Desalination*, 348 (2014) 82–88.
- [14] M. Safarpour, A. Khataee, V. Vatanpour, Thin film nanocomposite reverse osmosis membrane modified by reduced graphene oxide/TiO₂ with improved desalination performance, *J. Membr. Sci.*, 489 (2015) 43–54.
- [15] M. Ionita, E. Vasile, L.E. Crica, S.I. Voicu, A.M. Pandelescu, S. Dinescu, L. Predoiu, B. Galateanu, A. Hermenean, M. Costache, Synthesis, characterization and in vitro studies of polysulfone/graphene oxide composite membranes, *Composites Part B*, 72 (2015) 108–115.
- [16] S.-C. Shiu, J.-L. Tsai, Characterizing thermal and mechanical properties of graphene/epoxy nanocomposites, *Composites Part B*, 56 (2014) 691–697.
- [17] B.M. Ganesh, A.M. Isloor, A.F. Ismail, Enhanced hydrophilicity and salt rejection study of graphene oxide-polysulfone mixed matrix membrane, *Desalination*, 313 (2013) 199–207.
- [18] L. Yu, Y. Zhang, B. Zhang, J. Liu, H. Zhang, C. Song, Preparation and characterization of HPEI-GO/PES ultrafiltration membrane with antifouling and antibacterial properties, *J. Membr. Sci.*, 447 (2013) 452–462.
- [19] H.-R. Chae, J. Lee, C.-H. Lee, I.-C. Kim, P.-K. Park, Graphene oxide-embedded thin-film composite reverse osmosis membrane with high flux, anti-biofouling, and chlorine resistance, *J. Membr. Sci.*, 483 (2015) 128–135.
- [20] L. He, L.F. Dumée, C. Feng, L. Velleman, R. Reis, F. She, W. Gao, L. Kong, Promoted water transport across graphene oxide-poly(amide) thin film composite membranes and their antibacterial activity, *Desalination*, 365 (2015) 126–135.
- [21] Y.P. Tang, D.R. Paul, T.S. Chung, Free-standing graphene oxide thin films assembled by a pressurized ultrafiltration method for dehydration of ethanol, *J. Membr. Sci.*, 458 (2014) 199–208.
- [22] M. Shibuya, M. Yasukawa, T. Takahashi, T. Miyoshi, M. Higa, H. Matsuyama, Effect of operating conditions on osmotic-driven membrane performances of cellulose triacetate forward osmosis hollow fiber membrane, *Desalination*, 362 (2015) 34–42.
- [23] P. Song, X. Zhang, M. Sun, X. Cui, Y. Lin, Synthesis of graphene nanosheets via oxalic acid-induced chemical reduction of exfoliated graphite oxide, *RSC Adv.*, 2 (2012) 1168–1173.
- [24] M. Hu, B. Mi, Enabling graphene oxide nanosheets as water separation membranes, *Environ. Sci. Technol.*, 47 (2013) 3715–3723.
- [25] X. Wang, X. Wang, P. Xiao, J. Li, E. Tian, Y. Zhao, Y. Ren, High water permeable free-standing cellulose triacetate/graphene oxide membrane with enhanced antibiofouling and mechanical properties for forward osmosis, *Colloids Surf., A*, 508 (2016) 327–335.
- [26] S. Xia, L. Yao, Y. Zhao, N. Li, Y. Zheng, Preparation of graphene oxide modified polyamide thin film composite membranes with improved hydrophilicity for natural organic matter removal, *Chem. Eng. J.*, 280 (2015) 720–727.
- [27] S. Bano, A. Mahmood, S.-J. Kim, K.-H. Lee, Graphene oxide modified polyamide nanofiltration membrane with improved flux and antifouling properties, *J. Mater. Chem. A*, 3 (2015) 2065–2071.
- [28] V. Freger, Nanoscale heterogeneity of polyamide membranes formed by interfacial polymerization, *Langmuir*, 19 (2003) 4791–4797.
- [29] R. Ding, H. Zhang, Y. Li, J. Wang, B. Shi, H. Mao, J. Dang, J. Liu, Graphene oxide-embedded nanocomposite membrane for solvent resistant nanofiltration with enhanced rejection ability, *Chem. Eng. Sci.*, 138 (2015) 227–238.
- [30] Y. Zhang, S. Zhang, T.-S. Chung, Nanometric graphene oxide framework membranes with enhanced heavy metal removal via nanofiltration, *Environ. Sci. Technol.*, 49 (2015) 10235–10242.

- [31] L. Shen, S. Xiong, Y. Wang, Graphene oxide incorporated thin-film composite membranes for forward osmosis applications, *Chem. Eng. Sci.*, 143 (2016) 194–205.
- [32] B. Mi, M. Elimelech, Chemical and physical aspects of organic fouling of forward osmosis membranes, *J. Membr. Sci.*, 320 (2008) 292–302.
- [33] Y. Wang, R. Ou, H. Wang, T. Xu, Graphene oxide modified graphitic carbon nitride as a modifier for thin film composite forward osmosis membrane, *J. Membr. Sci.*, 475 (2015) 281–289.

Supplementary material

Table S1
Water fluxes of F0 and F4 membranes before and after 300 min filtration test

Membrane	Duplicate samples	Initial water flux (LMH)	Final water flux (LMH)
F0 in AL-FS mode	No. 1	5.67	5.26
	No. 2	5.83	5.38
	No. 3	5.77	5.29
	No. 4	5.64	5.21
F0 in AL-DS mode	No. 1	7.40	6.40
	No. 2	7.42	6.43
	No. 3	7.39	6.52
	No. 4	7.35	6.47
F4 in AL-FS mode	No. 1	9.32	8.16
	No. 2	9.20	8.23
	No. 3	9.20	8.33
	No. 4	9.17	8.28
F4 in AL-DS mode	No. 1	11.78	11.02
	No. 2	12.48	11.14
	No. 3	11.96	10.45
	No. 4	12.64	10.85

The FO operating conditions: 2 mol·L⁻¹ NaCl solution as the draw solution, 10 mmol·L⁻¹ NaCl solution as the feed solution, and the cross-flow rate was 20 L·h⁻¹.